African monsoon enhancement during the penultimate glacial period (MIS 6.5 ~ 170 ka) and its atmospheric impact

Amandine Tisserand,[1,2,3] Bruno Malaizé,[1] Elsa Jullien,[1] Sébastien Zaragosi,[1] Karine Charlier,[1] and Francis Grousset[1]

Received 1 April 2008; revised 13 February 2009; accepted 9 April 2009; published 20 June 2009.

[1] A reconstruction of northwest African summer monsoon strength during the cold marine isotopic stage (MIS) 6 indicates a link to the seasonal migration of the Intertropical Convergence Zone (ITCZ). High-resolution studies of eolian dust supply and sea surface temperature recorded in marine core MD03-2705, on the Mauritanian margin, provide a better understanding about the penultimate glacial history of northwestern African aridity/humidity and upwelling coastal activity. Today, site MD03-2705 experiences increased upwelling and dust flux during the winter months, when the ITCZ is in a southerly position. Analyses of foraminifera isotopic composition suggest that during MIS 6.5 (180–168 ka) the average position of the ITCZ migrated north, marked by an increase in the strength of the summer monsoon, which decreased eolian dust transport and the coastal upwelling activity. The northward migration is in phase with a specific orbital combination of a low precessional index with a high obliquity signal. High-resolution analysis of stable isotopes (δ^{18}O and δ^{13}C) and microscale resolution geochemical (Ti/Al and quartz grain counts) determinations reveal that the transition between monsoonal humid (MIS 6.5) and dry (MIS 6.4) conditions has occurred in less than 1.3 ka. Such rapid changes suggest a nonlinear link between the African monsoonal rainfall system and environmental changes over the continent. This study provides new insights about the influence of vegetation and oceanic temperature feedbacks on the onset of African summer monsoon and demonstrates that, during the penultimate glacial period, changes in tropical dynamics had regional and global impacts.

Citation: Tisserand, A., B. Malaizé, E. Jullien, S. Zaragosi, K. Charlier, and F. Grousset (2009), African monsoon enhancement during the penultimate glacial period (MIS 6.5 ~ 170 ka) and its atmospheric impact, *Paleoceanography*, *24*, PA2220, doi:10.1029/2008PA001630.

1. Introduction

[2] The northwest coast of Africa is strongly influenced by the monsoon system, because of the seasonal cycle in the location of the ITCZ [e.g., *Gasse*, 2000]. In the Northeast equatorial Atlantic Ocean, shifts in the ITCZ cause strong seasonal variations in sea surface hydrology, with the monsoon signature expressed primarily by changes in the sea surface temperature (SST) [e.g., *deMenocal et al.*, 2000; *deMenocal*, 2004]. When the ITCZ moves south, stronger monsoonal winter winds result on the African northwest coast [*Matthewson et al.*, 1995; *Martinez et al.*, 1999], intensifying coastal upwelling near the coast of Mauritania [*Van Camp et al.*, 1991], with a latitudinal extent of this upwelling depending on the amount of southward ITCZ migration (Figure 1).

[3] Previous studies on marine sedimentary records from the equatorial Atlantic Ocean have revealed a clear Milankovitch precessional forcing on the monsoon [*Prell and Kutzbach*, 1987; *Molfino and McIntyre*, 1990; *deMenocal*, 1995; *Schneider et al.*, 1997]. *Tuenter et al.* [2003] have also shown a significant contribution of the obliquity signal on the African summer monsoon using a coupled atmosphere/ocean/vegetation model of intermediate complexity (CLIMBER-2). Recently, a high-resolution study of a marine core off the coast of Somalia, in the Socotran basin, suggests that the obliquity signal is tied to changes in the summer monsoon, as recorded off the East coast of Africa during the penultimate glacial period [*Malaizé et al.*, 2006].

[4] Several terrestrial and marine studies of the Mediterranean basin have focused on marine isotope stage (MIS) 6 (ca. 185 and 135 ka) [*Rossignol-Strick*, 1983; *Ayalon et al.*, 2002; *Bard et al.*, 2002]. High-latitude glacial conditions during MIS 6 are characterized by the development of a large ice sheet over the northern Europe [*Imbrie et al.*, 1984; *Vostok Project members*, 1995; *Jouzel et al.*, 2007]. However, MIS 6 conditions in the tropics, where the atmospheric hydrology was more active with substantial African monsoons, appear different than during the last glaciation [*Rossignol-Strick*, 1985; *Mélières et al.*, 1997; *Rossignol-Strick and Paterne*, 1999]. Moreover, the eastern part of the Mediterranean Sea includes a sapropel layer (S6), which developed under glacial conditions, identified by pollen and faunal assemblages that differ from the interglacial sapropel conditions [*Rossignol-Strick*, 1983, 1985; *Cheddadi and Rossignol-Strick*, 1995]. According to *Ayalon et al.* [2002] and on the basis of oxygen and carbon isotopes composition of Soreq Cave speleothems, hydrological activity increased

[1]Université Bordeaux 1, EPOC, UMR5805, CNRS, Talence, France.
[2]Department of Earth Sciences, University of Bergen, Bergen, Norway.
[3]Bjerknes Centre for Climate Research, Bergen, Norway.

0883-8305/09/2008PA001630

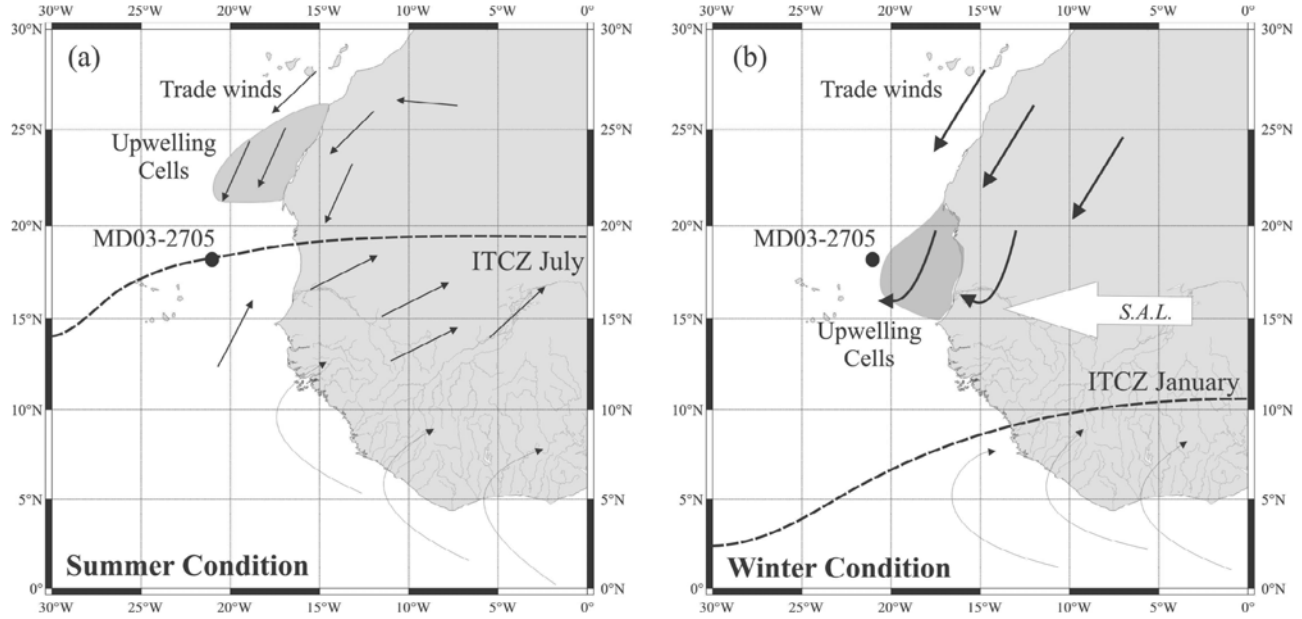

Figure 1. Location of core MD03-2705 (closed circles) and oceanic and atmospheric circulation in the northwestern African margin during (a) summer and (b) winter. The light gray area represents the upwelling cells. Dashed lines represent the present-day location of ITCZ in the Northern Hemisphere (adapted from *Gasse* [2000] and *Jullien et al.* [2007], with permission from Elsevier, and from *Nicholson* [1996], with permission). Light arrows represent the high-altitude Saharan air layer (SAL), and the dark arrows represent the low-altitude NE and SE trade winds (adapted from *Gasse* [2000] and *Ratmeyer et al.* [1999], with permission from Elsevier). The thickness of the dark arrows represents the strength of trade winds.

in Israel between 178 and 152 ka and records reveal a summer monsoon enhancement, with a northward displacement of the ITCZ during the MIS 6.5, in phase with a specific orbital configuration (low precession with high obliquity values) [*Ayalon et al.*, 2002].

[5] Although MIS 6 is distinguished by wet conditions, it may be considered as analogous to the three marine isotope stages of last glaciation (MIS 4, 3 and 2). The entire stage 6 presents conditions as cold as during the last glacial period. Meanwhile, the results of *Ding et al.* [1999] using high-resolution loess records in China suggest that millennial-scale climatic oscillations occurred during the penultimate glaciation as well as during the last glaciation. MIS 6 is marked by stadial and interstadial periods and it appears that the monsoon-desert system over northern China was relatively more stable during interstadial periods than stadial periods.

[6] Past studies have pointed out the link between tropical hydrological changes and millennial-scale climate perturbations [*Sirocko et al.*, 1996; *Ivanochko et al.*, 2005; *Weldeab et al.*, 2007; *Wang et al.*, 2008]. A multiproxy reconstruction of the Arabian Sea summer monsoon has suggested increased monsoon influence during warm D-O interstadials and decreased monsoon influence during cold stadials, implying a reconfiguration of tropical convection. These changes affected the atmospheric concentration and latitudinal extent of water vapor. Stadial/interstadial climate changes are recorded in subboreal and temperate regions and this large-scale impact could be perpetuated and amplified by a tropical phenomenon such as the monsoon [*Ivanochko et al.*, 2005]. The latitudinal extent of the Intertropical Convergence Zone (ITCZ) (e.g., southward migration during stadials and northward migration during interstadials) is a natural mode of variability to consider if the tropics are involved [*Ivanochko et al.*, 2005; *Jullien et al.*, 2007].

[7] Even if the setting of the monsoon system during MIS 6.5 might not have occurred at millennial times scale, one can still wonder about the link between the displacement of ITCZ and wet conditions recorded on the northwestern coast of Africa.

[8] In this paper, we focus on the relevant climatic mechanisms that might influence multiproxy records off the northwestern African area. As strong changes in monsoon and/or precipitation intensity have been observed during MIS 6.5 by others [e.g., *Rossignol-Strick*, 1983; *Cramp and O'Sullivan*, 1999; *Rossignol-Strick and Paterne*, 1999; *Bard et al.*, 2002; *Malaizé et al.*, 2006], this investigation will focus on marine isotopic stage 6.5 and on the transition to substage 6.4. We will investigate the notion that the northward migration of the ITCZ during warm and humid substage and the southward migration of the ITCZ while moving to a colder period [*Ivanochko et al.*, 2005] can be applied to the penultimate glacial period. We also examine the orbital forcing at the origin of such a latitudinal migration by comparing the West African marine record with an existing East African marine record [*Malaizé et al.*, 2006]. Finally, the implied changes to tropical circulation

are compared with those at the subpolar latitudes associated with the ice core records.

2. Environmental Setting

2.1. Atmospheric Regime and Dust Transport

[9] Modern climate conditions of the northwest African coast are governed by the seasonal monsoons dynamics associated with latitudinal shifts of the Intertropical Convergence Zone (ITCZ), which delineates dry subtropical air masses from the humid equatorial zone. Modern observations reveal a seasonal variation in humidity and continental precipitation. During the summer dry subtropical air is shifted northward to extreme North African latitudes as the ITCZ is located around 20°N (Figure 1). In the winter, the equatorward displacement of the ITCZ (5°N) causes a southward shift in dry subtropical air and is associated with the development of strong easterly Saharan air layer (SAL) winds. The southward shift of the ITCZ and development of winds causes dust transport from the Sahara. The dust plume is generally located between 15 and 25°N along an E-W axis over the tropical Atlantic Ocean.

[10] In past climates, changes in the interhemispheric temperature gradient, caused by Milankovitch-related insolation changes, might have induced a general southward displacement of the ITCZ during colder periods [*deMenocal*, 1995; *Broccoli et al.*, 2006; *Jullien et al.*, 2007] because cooling seems to occur preferentially in the Northern Hemisphere. The eolian dust flux record off West Africa is associated with variability of continental aridity in the Sahara and Sahel, which should also be related to the strength and/or position of the ITCZ [*Tiedemann et al.*, 1989; *Tiedemann*, 1991; *deMenocal*, 1995, 2004; *Jullien et al.*, 2007; *Mulitza et al.*, 2008].

2.2. Ocean Circulation

[11] The seasonal ITCZ migration exerts a strong influence on oceanic circulation. Northeast trade winds blow along the northwest African margin and induce surface water divergence. This drives the upwelling of cold, nutrient-rich waters that support high surface ocean productivity [*Mittelstaedt*, 1983]. In the eastern subtropical Atlantic Ocean, upwelling is most prevalent from November to February [*Mittelstaedt*, 1991] (Figure 1). The most intense perennial upwelling occurs off Cape Blanc near 20°N, where the southward flow of North Atlantic Central Water (NACW) meets less saline and nutrient-rich South Atlantic Central Water (SACW) flowing northward at depths between 150 and 600 m. Middepth waters provide source water for the upwelling [*Hughes and Barton*, 1974; *Martinez et al.*, 1999].

2.3. Strategy

[12] The purpose of this study is to interpret changes in the upwelling coastal records using the sea surface temperature (SST), a paleoproductivity proxy (planktonic $\delta^{13}C$) and continental aridity records (eolian dust supply), as tracers of ITCZ movement and monsoon enhancement. A well-dated high-resolution marine climate archive (MD03-2705) from the eastern tropical Atlantic under the direct influence of the ITCZ and associated to oceanographic circulation variability, is ideally situated to provide insight into the monsoon history during glacial periods in general and during MIS 6 in particular (Figure 1). For this purpose, we focus on $\delta^{18}O$ and $\delta^{13}C$ measurements to infer changes in water mass characteristics and we use Ti/Al ratio and quartz grain counts as proxies for eolian transport.

3. Material and Methods

[13] The 37 m MD03-2705 core (18°05,81'N; 21°09,19'W) was retrieved in the eastern tropical Atlantic Ocean. The core was collected during the MD134/PICABIA cruise on board the R/V *Marion Dufresne* (IPEV) (Figure 1). This core is taken from a seamount at around 3000 m of water depth roughly 500 km offshore. Consequently, the setting collects essentially hemipelagic sediments and is not disturbed by turbidites or contourites [*Moyes et al.*, 1979; *Weaver et al.*, 2000; *Holz*, 2004]. The core is situated at the northern winter limit of the Saharan dust plume [*Husar et al.*, 1997] and is swept by the dust winds during the summer.

[14] Using onboard magnetic susceptibility data (J.-L. Turon, PICABIA technical report, unpublished, 2003) and carbonate content, it is determined that core MD03-2705 covers the last 1.2 Ma, as far as marine isotopic stage (MIS) 36 (Malaizé et al., manuscript in preparation, 2009). The reflectance parameters measured along the core facilitated the identification of the MIS 6 section between 700 and 1020 cm. Sediment descriptions and SCOPIX [*Migeon et al.*, 1999] radioscopic analyses for this MIS 6 interval reveal continuous sedimentation. We sampled this interval for stable isotopic analysis at a resolution of 10 cm, which represents about 2500 years of sedimentation. The age model employed is discussed in the section 4 of this paper.

[15] In addition to hemipelagic sediments, there is a nonnegligible contribution from eolian sources coming from the Sahara/Sahel regions [*Jullien et al.*, 2007]. A terrigenous fraction transported by the Saharan air layer (SAL, e.g., Figure 1) winds is characterized by clay minerals and silt-sized quartz. The hemipelagic sediments are characterized by a large biogenic calcareous fraction, composed of foraminifera and coccoliths. According to *deMenocal et al.* [2000] and *Adkins et al.* [2006], the biogenic opal fraction is less than 5–7% in this area and varies between 2 and 3%. The opal supply is therefore considered as negligible.

[16] *Adkins et al.* [2006] have recently shown for the last 15 ka at the site ODP 658C, which is nearby MD03-2705, that the variations in terrigenous percentage are generally the same as the accumulation flux curve, on the basis of the excess ^{230}Th normalization. The terrigenous percentage record is therefore a reliable indicator of the abruptness and timing of the aridity/wet North African history [*deMenocal et al.*, 2000; *Adkins et al.*, 2006]. However, the carbonate percentage is significantly different from the carbonate-normalized flux. Consequently, the carbonate percentage highlights the dilution history by continental input and it should not be used as a proxy of calcareous paleoproductivity.

[17] Given a negligible biogenic opal contribution [*deMenocal et al.*, 2000], only the calcareous biogenic fraction and terrigenous particles are considered as sediment components. According to the previous assuming [*Adkins et al.*, 2006], the following relationship is used [*Jullien et al.*, 2007]:

$$\%\ \text{Terrigenous} = 100\% - \%\ \text{Carbonate}(\%CaCO_3).$$

[18] This equation is based on essentially a dilution equation between the two main components at our site. Even if the terrigenous percentage and flux shapes are similar in a neighboring core [*Adkins et al.*, 2006], it makes us wonder how the geochemical changes vary. This relation stays valid assuming that there is no change in carbonate preservation and terrigenous carbonate provision. Carbonate is not representative of the main components of terrigenous material with less than $\sim$ 10% calcite in ODP 658C site [e.g., *Glaccum and Prospero*, 1980]. According to *Beltagy et al.* [1972] and *Jullien et al.* [2007], the area is influenced by eolian terrigenous sources, as Saharan dusts seem to be mainly composed by aluminosilicates and mostly quartz grains, and terrigenous carbonate contributions are negligible. The detailed work on the samples suggests that the planktonic and benthic shell foraminifera were not dissolved. The site is situated close to a coastal upwelling area and under the control of the Saharan dust input. Consequently, it can be controlled by the changes in dust input and the productivity. *Guichard et al.* [1999] have studied the variability of the Mauritanian coastal upwelling signal and it seems that the main change in paleoproductivity occurred during the glacial periods and especially during MIS 2. However, organic matter fluxes are not important in some events of stage 6 [*Guichard et al.*, 1999]. In the MD03-2705 site, the $CaCO_3$ percentage shape seems to be in opposition to planktonic $\delta^{13}C$. It suggests that the $CaCO_3$ percentage is not influenced by the surface productivity. To rely on this assumption, *Adkins et al.* [2006] suggest that the $CaCO_3$ percentage shape is different from the $CaCO_3$ fluxes curve. It seems obvious that the carbonate sedimentation is under a climatic control despite a complicated approach of the proxy, which depends on several external factors (e.g., oceanic circulation, surface productivity, etc.). Future works based on the paleo-pH estimations will help to quantify the carbonate dissolution effect in northwestern Africa.

[19] In the MD03-2705 core, Ca is mainly derived from biogenic $CaCO_3$ because the terrigenous provision is composed mostly of quartz [*Jullien et al.*, 2007]. The Ca content is determined directly from the volumetric method with Bernard calcimeter [*Huelsemann*, 1966; *Muller and Gatsner*, 1971] by measuring the CO_2 extracted by the acidification of the bulk sediment and the CO_2 content stoichiometrically converted back into $CaCO_3$ amount (%). To improve the resolution of the $CaCO_3$ content measurements, we have calibrated the Ca obtained through X-ray fractionation (XRF) data using a few measurements from the volumetric method. Representative high, low and medium points from the XRF data are used to make the calibration.

[20] In addition, aluminum counts are useful proxies to monitor changes in aridity of the source areas. *Matthewson et al.* [1995] proposed that aluminum concentration is taken as proxy of dust input in the northwest African margin because it is incorporated into the fine-grained wind clays. The net counts for aluminum were not expressed as percentages because not all major elements have been measured using X ray. Results are presented in aluminum counts and represent the variations of the aluminosilicate mineral fraction. It should help to understand the terrigenous supply associated with the terrigenous percentage calculation, although changes in percentage of Al are affected by dilution.

[21] Thin sections of the core have been produced to obtain a microscale resolution record of "dustiness." Microscope observations of the 10 cm long thin sections of impregnated sediments selected from well preserved and representative sedimentary limit were performed using a fully automated LEICA DM6000 B Digital Microscope. This method has been recently detailed by *Zaragosi et al.* [2006].

[22] Observations were focused on three thin sections of impregnated sediments during the specific substadials MIS 6.5 and MIS 6.4. Direct observations and quartz grain counts of shape and size parameters are the main products of this new, highly precise tool.

[23] Benthic (*Planulina wuellerstorfi*) and planktonic (*Globigerinoides ruber*) foraminifera are associated with the 250–315 μm grain size fraction. The preparation of each aliquot of 5–7 specimens for *G. ruber* and 2–3 specimens for *P. wuellerstorfi*, representing a mean weight between 50 and 100 μg, has been carried out using a micromass multiprep autosampler which performed individual acid dissolution using phosphoric acid for each sample.

[24] The $^{18}O/^{16}O$ ($\delta^{18}O$) and $^{13}C/^{12}C$ ($\delta^{13}C$) ratios, expressed in ‰ versus Pee Dee Belemnite (PDB), were measured at the UMR 5805 EPOC of Bordeaux I University, on a Micromass Optima© mass spectrometer. The carbon dioxide gas extracted was analyzed against PDB, defined with respect to NBS19 calcite standard, which is used as an international reference standard.

[25] Measurements of major elements on core MD03-2705 were performed on the bulk sediments with the Bremen cortex X-ray fluorescence (XRF) [*Jansen et al.*, 1998] at 1 cm resolution step during the MIS 6 section of the core. Among the 10 measured major elements, we focus on Ti, Ca, Al, Si and on the Ti/Al and Si/Al ratio in particular. The concentration of Al, in common igneous and metamorphic rock sources, is relatively invariable and minimally affected by weathering [*Calvert et al.*, 2001]. Therefore, normalization of element contents to Al can be used to remove the effects of differential dilution of the biogenous and authigenic components of marine sediments by the aluminosilicate fraction so that changes in the composition of the lithogenous material can be discerned. Ti is present in heavy grains generally associated with coarser grained sediments. Ti/Al is considered to be a useful proxy for wind intensity [*Boyle*, 1983]. Given the location of the core relative to the source region for the dust, Ti/Al ratio marks the strength of continental winds. According to *deMenocal et al.* [2000] the

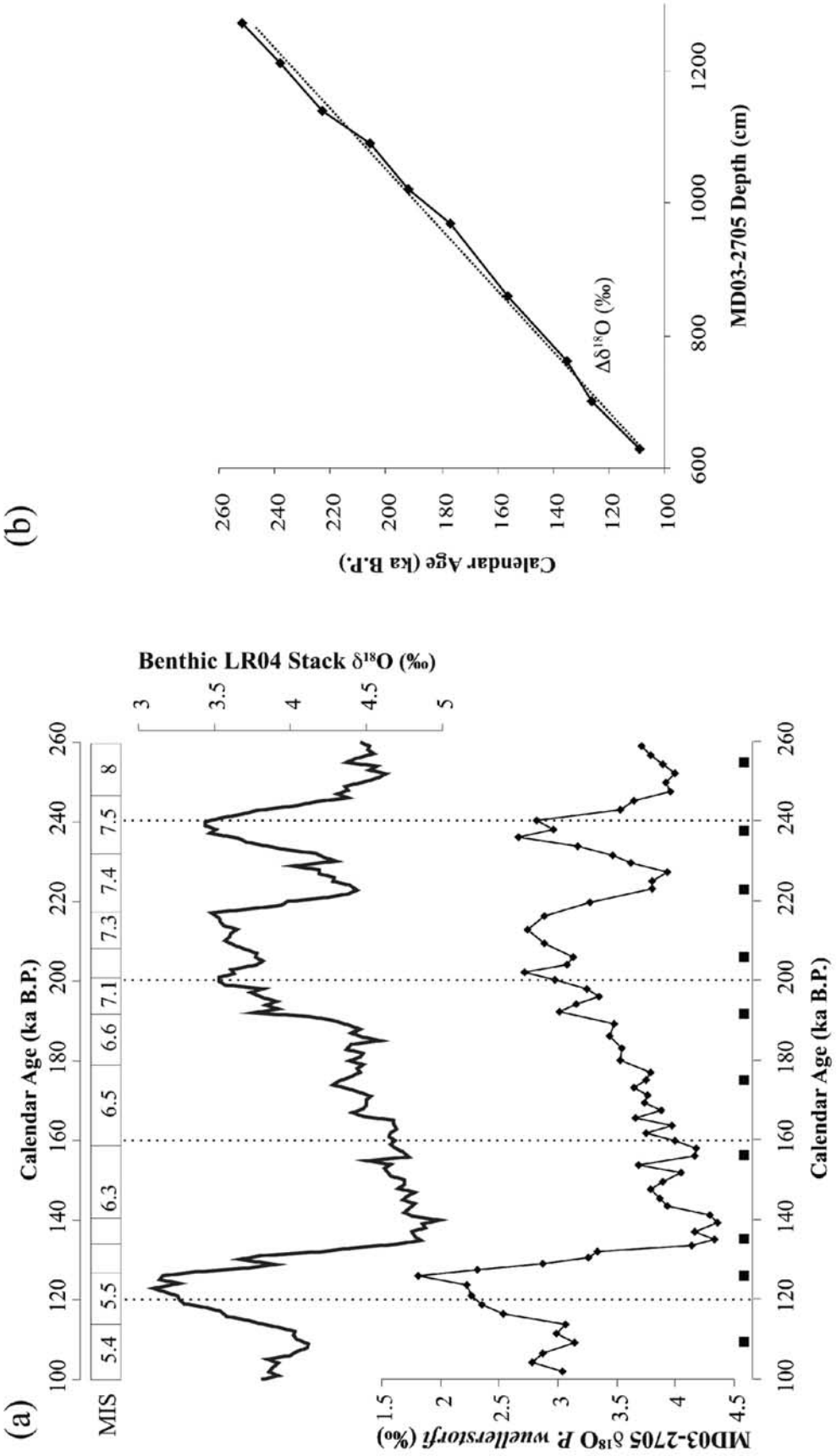
(a)
Benthic LR04 Stack δ18O (‰)
3
3.5
4
4.5
5
MIS
5.4
5.5
6.3
6.5
6.6
7.1
7.3
7.4
7.5
8
Calendar Age (ka B.P.)
100
120
140
160
180
200
220
240
260
MD03-2705 δ18O P. wuellerstorfi (‰)
1.5
2
2.5
3
3.5
4
4.5
(b)
Calendar Age (ka B.P.)
Δδ18O (‰)
MD03-2705 Depth (cm)
600
800
1000
1200

Figure 2

Table 1. Control Points Used to Adjust the Age Model of Core MD03-2705 Benthic Record to the Benthic Stack of *Lisiecki and Raymo* [2005]

Isotopic Events	Ages (ka)	Depth of Control Points (cm)	Sedimentary Rates (cm/ka)
5.4	109	630	
5.5–6.1	126	700	4.12
6.1–6.2	135	760	6.67
6.4	156	860	4.76
6.5	177	970	5.24
6.6–7.1	192	1020	3.34
7.2	206	1090	5
7.4	223	1140	2.94
7.5	238	1210	4.67
8.2	252	1270	4.29

contribution of biogenic opal is negligible and Si/Al ratio is considered o be a proxy of changes in aluminosilicates.

4. Results

4.1. Stratigraphy of Core MD03-2705

[26] *Jullien et al.* [2007] built an age model for the last 75 ka (the seven upper meters of MD03-2705) using the $\delta^{18}O/\delta^{13}C$ record and AMS ^{14}C ages. In this paper, the age model of *Jullien et al.* [2007] is extended to the penultimate climatic cycle. The oxygen isotope record of *P. wuellerstorfi* (representing ice volume changes) is compared with the benthic stack LR04 [*Lisiecki and Raymo*, 2005] (Figure 2 and Table 1). Using the Analyseries program developed by *Paillard et al.* [1996], we have defined 10 age control points for the time period covering MIS 5e–MIS 6–MIS 7 which are listed in Table 1 and shown in Figure 2. We have focused on age control points between the high benthic stack $\delta^{18}O$ and the low benthic stack $\delta^{18}O$ values. We have chosen two additional control points associated with isotopic events 6.4 and 6.5. The correlation coefficient between the *P. wuellerstorfi* and benthic stack curves is 0.93 and the mean accumulation rate is about 4 cm/ka, presenting no "step-like" shape over the studied time period. The uncertainty due to measurements and confirmed by replicate analysis is less than 0.13 (2σ) for benthic $\delta^{18}O$ record. The 10 cm sampling interval corresponds to a mean temporal resolution of 2.5 ka.

4.2. Benthic and Planktonic Foraminifera

[27] Figure 3 shows the $\delta^{18}O$ record of benthic foraminifera *P. wuellerstorfi* and the $\delta^{18}O$ record of planktonic foraminifera is marked by a depletion of 0.3 per mil between 185 and 175 ka and a enrichment of 0.7 per mil starting at 175 ka and ending at 160 ka (Figure 3b). Three hypotheses could be proposed to explain such changes in the oxygen isotopic ratios: (1) global changes in the $\delta^{18}O$ of the ocean, caused by global sea level changes that result from changes in the mass of continental ice sheets; (2) SST changes, and (3) sea surface salinity (SSS) changes. During MIS 6.5, changes in benthic $\delta^{18}O$ values are of about 0.35 per mil, which represent 25% of the total glacial/interglacial $\delta^{18}O$ change in the benthic curve. Regarding the first hypothesis, the amount of variation in the benthic $\delta^{18}O$ record is insufficient to explain the entire isotopic depletion signal in the planktonic curve. Therefore, the remaining difference is probably linked to other sea surface changes. The area of study is currently affected by SST variations while the SSS remains almost constant at around ~36‰ all year long [*Levitus and Boyer*, 1994; *Levitus et al.*, 1994]. The site does not seem to be significantly influenced by freshwater discharge, because the site is located roughly 500 km from the continent and there are no major drainage basins in the vicinity of the core. The summer monsoonal rainfall on Mauritania offshore is in average 15–20 mm during the summer monsoon (June to August, see http://jisao.washington.edu) and it appears weak compared to a typical monsoonal rainfall where the monsoonal activity records over 300 mm per month [*Murgese et al.*, 2008]. Consequently, the West African rainfall does not generate a strong seasonal salinity contrast at the sea surface. The Senegal drainage basin is located further south and the effect of the trade winds prevents surface freshwater from flowing northward into the vicinity of the core. As SSS changes seem negligible at present time, we can suppose that the third hypothesis can be disregarded. We therefore consider the difference between the benthic $\delta^{18}O$ and planktonic $\delta^{18}O$ (here after $\Delta\delta^{18}O$) as roughly representative of SST in the vicinity of the core.

[28] The $\Delta\delta^{18}O$ time series shows a drop of about 0.6 per mil between 175 ka and 160 ka during isotopic substage 6.5 (Figure 4). Converted to a temperature difference, this represents an increase of about 2.4°C (mean calibration value) [*O'Neil et al.*, 1969; *Duplessy et al.*, 1991; *Kim and O'Neil*, 1997; E. Michel, personal communication, 2006].

[29] Measurements of $\delta^{13}C$ on planktonic foraminiferal species *G. ruber* have been conducted to estimate past surface productivity, which is linked to the strength of the Mauritanian upwelling. Results indicate a decline of planktonic $\delta^{13}C$ after 185 ka, with a minimum around 175 ka (Figure 4).

4.3. Elemental Measurements

[30] Measurements of the Ti/Al ratio and Al counts provide an estimate of past wind strength and terrigenous percentage (%) provides an estimate of the terrigenous flux (Figures 3 and 4) [e.g., *Adkins et al.*, 2006]. The MIS 6.5 exhibits low terrigenous concentrations (50–30%) and very low Ti/Al ratios (Ti is roughly equal to Al) associated with low Al counts.

[31] During interglacial periods (substages 5.5 and 7.1), the terrigenous fraction is low (30–40%) indicating the dominance of the biogenic ($CaCO_3$ supply) and fine par-

Figure 2. (a) The Mauritanian margin benthic isotopic record ($\delta^{18}O$) (bottom curve) and the benthic stack LR04 of *Lisiecki and Raymo* [2005] (top curve). The isotopic events used as control points are numbered following *Lisiecki and Raymo* [2005] and indicated by squares. (b) The age model scale used (line with diamonds). The dotted line corresponds to the continuous accumulation rate curve.

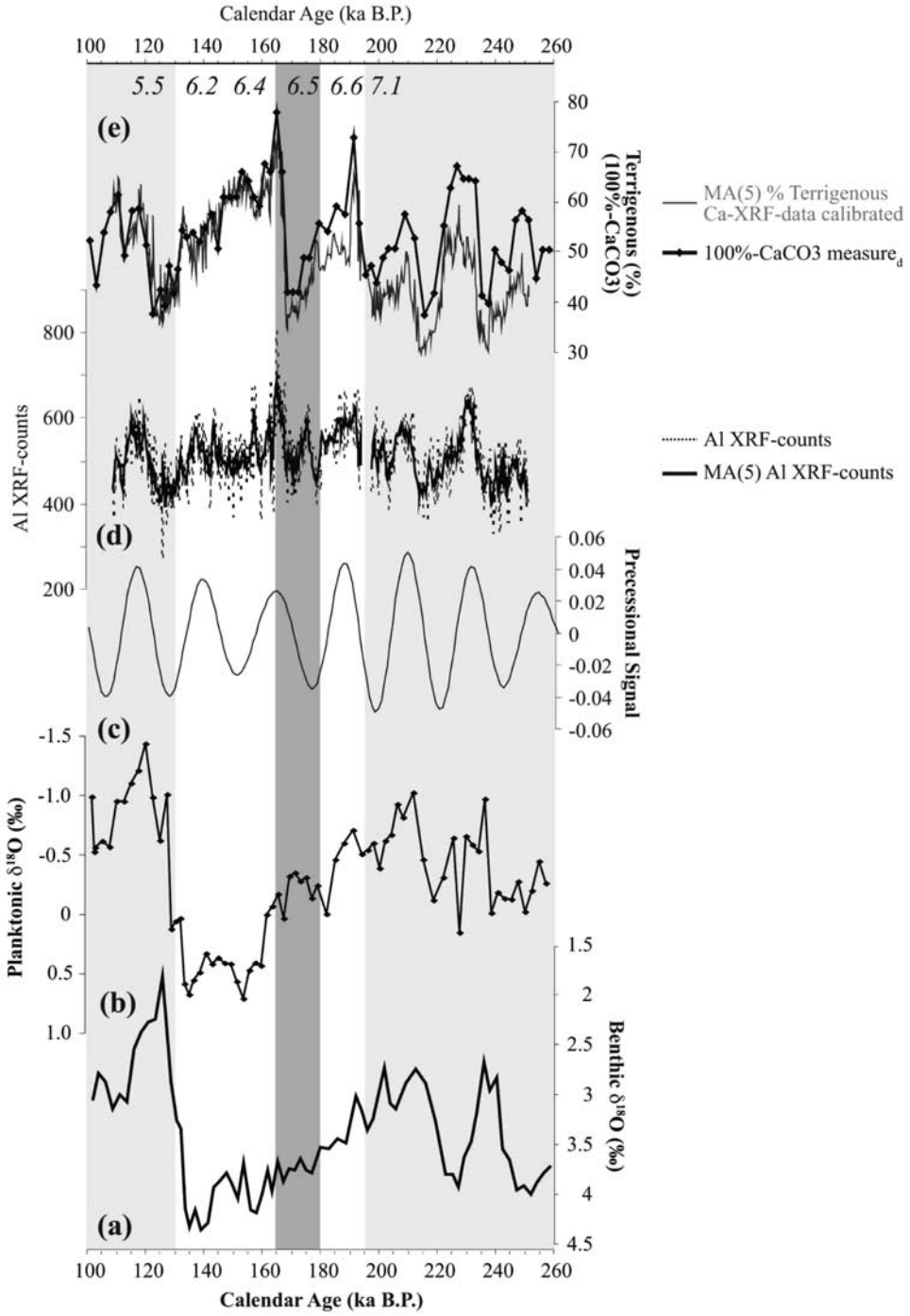

Figure 3. Mauritanian stratigraphy and dusty record of MIS 5.5–MIS 6–MIS 7: (a) $\delta^{18}O$ record of *P. wuellerstorfi* benthic foraminifera, (b) $\delta^{18}O$ record of *G. ruber* planktonic foraminifera, (d) Al XRF counts variations, and (e) terrigenous variations (percent) obtained from the bulk sediment of MD03-2705. The line with black diamonds shows terrigenous percentage obtained by $CaCO_3$ rate directly measured by gasometric method, and the gray line represents the five-sample moving average (MA) of terrigenous percentage obtained by $CaCO_3$ calibrated from the data of Ca XRF. (c) The precessional signal curve shows a good correlation with terrigenous supply (percentage and Al counts).

ticles (low Ti/Al ratio). During the glacial stage 6, the terrigenous fraction is high (50–60%), with a maximum (70%) during MIS 6.4. Coarse particles (high Ti/Al) dominate during MIS 6.4, likely supplied by stronger winds as during other glacial periods. The terrigenous fraction dominance during MIS 6.4 is in contrast with conditions during MIS 6.5 episode. Dust abundances, comparable to intergla-

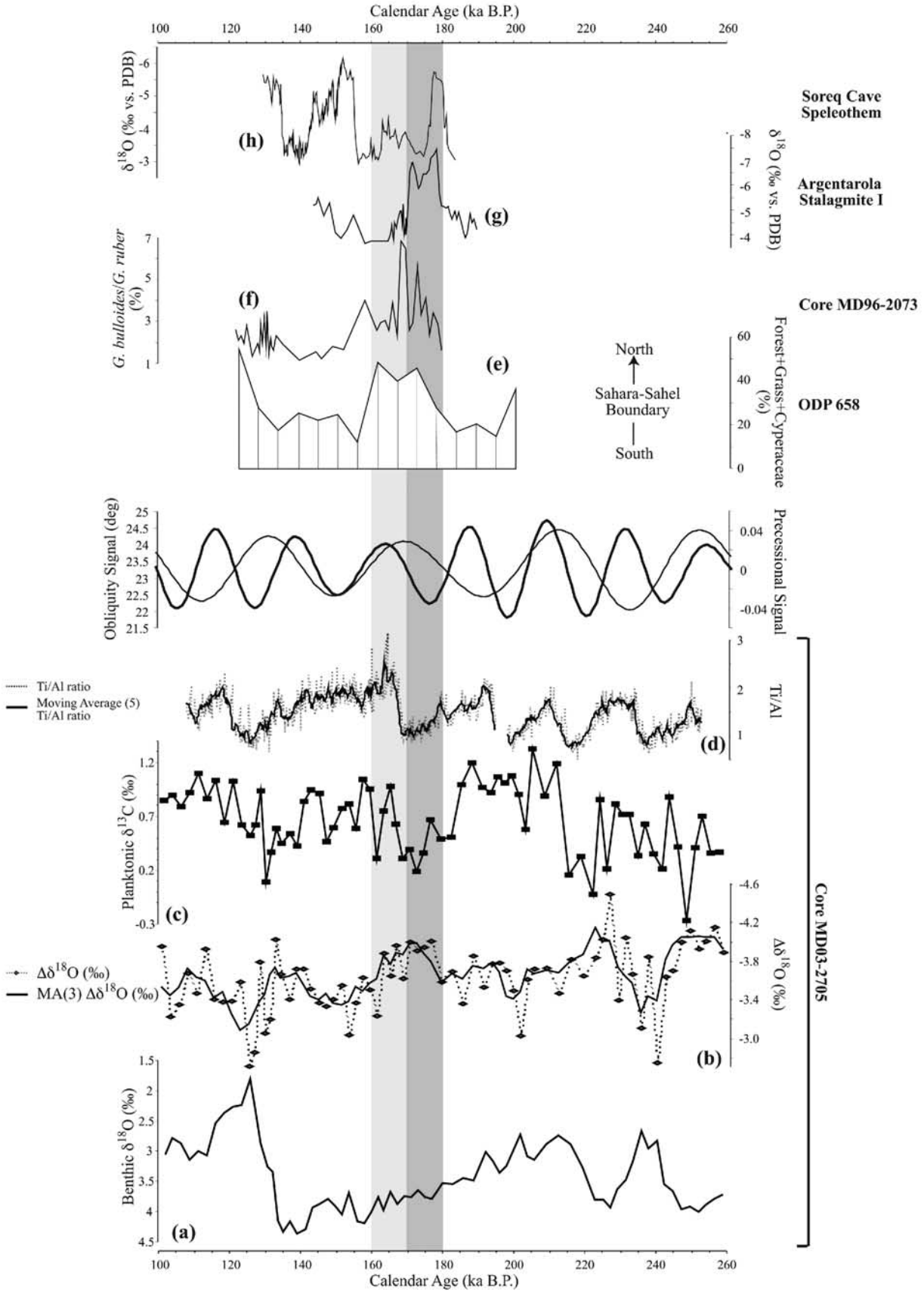
Calendar Age (ka B.P.)
100 120 140 160 180 200 220 240 260
δ18O (‰ vs. PDB)
(h)
Soreq Cave Speleothem
(g)
Argentarola Stalagmite I
G. bulloides/G. ruber (%)
(f)
(e)
Core MD96-2073
North
Sahara-Sahel Boundary
South
Forest+Grass+Cyperaceae (%)
ODP 658
Obliquity Signal (deg)
Precessional Signal
Ti/Al ratio
Moving Average (5) Ti/Al ratio
Ti/Al
(d)
Planktonic δ13C (‰)
(c)
Δδ18O (‰)
MA(3) Δδ18O (‰)
(b)
Benthic δ18O (‰)
(a)
Core MD03-2705

Figure 4

cial values, are around 30% and the particle mean size decreases (low Ti/Al ratio).

4.4. Microscale Study of Thin Sections: Ultrahigh Resolution

[32] Thin sections allow direct comparisons between wind strength proxies (Ti/Al ratio) and the eolian grain quantification (quartz) (Figure 5). Eolian grain size is between 30 and 40 μm, matching the mean grain size observed in present-day Mauritanian aerosols [*Grousset and Biscaye*, 2005] and in general agreement with eolian grain sizes cited in the literature [*Tsoar and Pye*, 1987]. The microscopic observation of the thin sections reveals a prominent "eolian" lamina (1 cm long) (Figure 5, right) and homogeneous, fractured lithic grains floating within a fine clay matrix. No preferred orientation for the grains was found. The eolian lamina represents a transition zone between the thin foraminifera facies and a facies composed of eolian grains with hardly any foraminifera (Figure 5, right). This eolian maximum lamina was deposited at around 168 ka. It suggests a unique period of large dust plume activity. The highest Ti/Al ratio in the core and the occurrence of lamina are observed during MIS 6.5–MIS 6.4 transition.

[33] Three main phases of "dusty" activity are observed (Figure 5, left).

[34] 1. During MIS 6.5 until 169 ka, there are fewer quartz grains and a relatively low Ti/Al and low Al counts.

[35] 2. From 169 to 168 ka, a large and sudden increase in deposits of eolian continental dust in the core, which is identifiable in the dusty lamina on the middle thin section in natural light, occurs in less than 1.3 ka during the transition between MIS 6.5 and MIS 6.4. The eolian dust delivery to the core reached a maximum intensity at around 168 ka.

[36] 3. From 167 ka, there is a moderate decrease in the number of quartz grains, but the Ti/Al ratio remains relatively high. The deviation between these two measurements is certainly due to two different dust grain populations. The dust input is not less than before but contains more grains of a smaller size, which are difficult to count. It could explain this deviation after 167 ka.

[37] Consequently, Ti/Al ratio can help us to interpret and define the limit of the new method. These results indicate that the indirect (Ti/Al ratio) and the direct (number of quartz grains) method to reconstruct continental wind strength are mostly in agreement. Further studies of MIS 6.4 should be carried out. Direct high-resolution observations of terrigenous sediments through the microscopic observation of thin layers have shown to be of great interest for the future studies.

5. Discussion

5.1. Evidence of Monsoon Climate in the Northwest Africa

[38] Evidence of increased summer monsoon-related precipitation during MIS 6.5 has been observed previously in paleorecords [e.g., *Rossignol-Strick*, 1983; *Bard et al.*, 2002]. Today, strong summer monsoon in the Northeast Atlantic Ocean is linked with increased sea surface temperatures (SST), caused by a northward displacement of the coastal upwelling cells away from site MD03-2705 (Figure 1). In core MD03-2705, the difference between planktonic and benthic foraminifera δ^{18}O shows a SST increase of about 2.4°C and the planktonic δ^{13}C reveals a decline in surface water productivity during MIS 6.5 in core MD03-2705 (Figure 4). During low-productivity periods, planktonic foraminifera incorporate more easily the ^{12}C isotope than the ^{13}C isotope, which results in a decrease of their δ^{13}C values [*Schneider et al.*, 1994]. This discrimination in favor of ^{12}C isotope shifts the δ^{13}C of organic matter toward values that are heavier than the initial inorganic carbon source [*Curry et al.*, 1988; *Mackensen and Bickert*, 1999]. The combination of these events could be reasonably linked to a decline in the Mauritanian upwelling during MIS 6.5. A low Ti/Al ratio suggests reduced wind strength and a decrease in the supply of terrigenous material from the African desert, which could be linked to an increase in humidity over the continent. All these results are consistent with a northward shift of the ITCZ during MIS 6.5.

[39] Climate change can modulate continental aridity and therefore eolian dust transport: during glacial periods a global increase of dust flux has been identified [*Petit et al.*, 1999; *Lambert et al.*, 2008]. During glacial substages (i.e., MIS 6.4 and MIS 6.6), the high Ti/Al ratio (>3) indicates the influence of stronger continental winds leading to the arrival of more frequent and heavier terrigenous particles to the Mauritanian margin compared to interglacial periods. A productivity increase associated with increased upwelling is observed during the same intervals (higher δ^{13}C values and lower SST). The glacial substages record increased continental aridity and stronger winds that are probably caused by an abrupt southward migration of the ITCZ, starting at around 168 ka, with a humid/arid transition which occurred in less than 1.3 ka. Decreased SSTs associated and increased productivity also suggest increased

Figure 4. Temporal distribution (between 100 and 260 ka B.P.) of different parameters. In the core MD03-2705, (a) the δ^{18}O record of benthic foraminifera, (b) the $\Delta\delta^{18}$O record (δ^{18}O *P. wuellerstorfi* benthic foraminifera minus δ^{18}O *G. ruber* planktonic foraminifera) used as sea surface temperature (SST) indicator, (c) the planktonic δ^{13}C (*G. ruber*), and (d) the Ti/Al ratio obtained from XRF data: the dotted line represents the Ti/Al ratio, and the bold dark line is a five-sample moving average of Ti/Al ratio. Comparison of our MD03-2705 results with (e) the pollen percentage diagram of selected plant taxa (forest, grass, and Cyperaceae) in the ODP 658 [*Dupont and Hooghiemstra*, 1989], (f) the abundance ratio of *G. bulloides*/*G. ruber* in the core MD96-2073 [*Malaizé et al.*, 2006], (g) the δ^{18}O Argentarola stalagmite on the Tyrrhenian coast of Italy [*Bard et al.*, 2002], and (h) the δ^{18}O Soreq Cave speleothem in Israel [*Ayalon et al.*, 2002]. The vertical dark gray band represents the MIS 6.5 episode and denotes the implied maximum monsoon-influenced period during MIS 6.5. The vertical light gray band represents the transition between MIS 6.5 and 6.4. Orbital parameters (obliquity and precessional) from 100 to 260 ka suggest the link with the monsoon system.

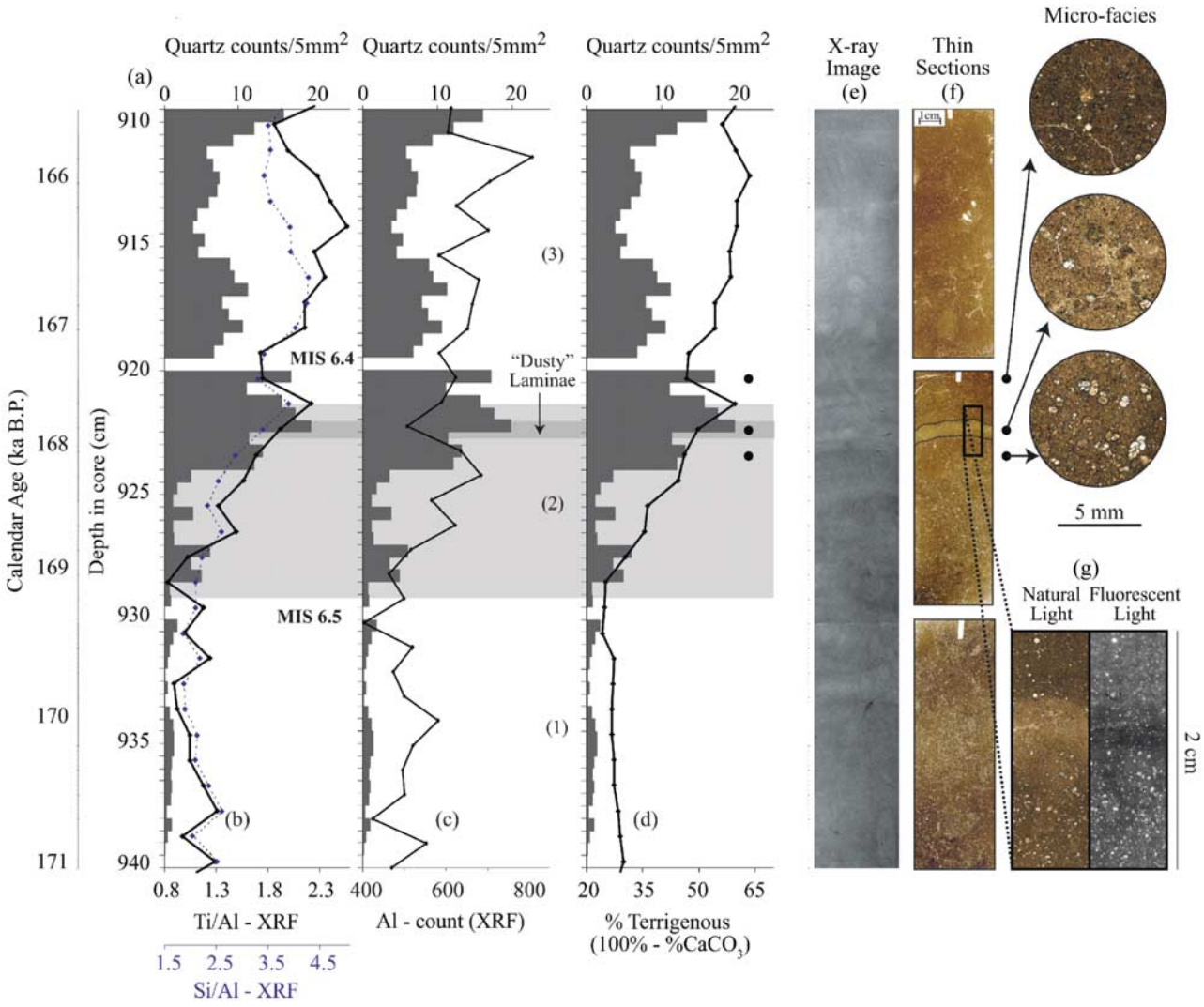

Figure 5. (left) Comparison between (a) the direct method for wind strength reconstruction and (b, c, d) the indirect methods for paleoclimatic records from core MD03-2705 between 171 and ~165 ka B.P. Figure 5a shows histogram counts of eolian quartz grains directly from the analyses of thin sections with a 5 mm^2 resolution (quartz counts per 5 mm^2), Figure 5b shows Ti/Al and Si/Al ratios obtained by the XRF method aluminum contents (XRF counts) (Figure 5c) and terrigenous fraction abundance (%) (Figure 5d). (right) (e) Variable-scale X-ray imagery, (f) thin sections of impregnated sediment microphotography of MD03-2705, and (g) a focused microphotography of dusty lamina in natural light and fluorescent light. The presence of microfacies microphotography before, during, and after the dusty lamina is noted with dark circles. The horizontal light gray band corresponds to the transition between MIS 6.5 and MIS 6.4, and the smaller horizontal dark gray band represents the width of dusty lamina in the thin section.

upwelling at the end of MIS 6.5, consistent with a southward migration of the ITCZ.

5.2. Are the Northwestern African "Monsoon" Dynamics Changes a Regional Manifestation of Equatorial Climate Variability?

[40] To determine the scale of changes observed during MIS 6.5 in core MD03-2705, our records are compared with other paleoclimatic records obtained from around North Africa (Figure 4). Comparisons are performed with results from a sediment core in the Arabian Sea [*Malaizé et al.*, 2006], with speleothem data from the Soreq Cave in Israel [*Ayalon et al.*, 2002] and the Argentarola cave in Italy [*Bard et al.*, 2002] and with continental pollen data from a sediment core situated in the Mauritanian margin [*Dupont and Hooghiemstra*, 1989] (e.g., Figure 6). Observations from core MD03-2705 suggest a northward migration of the mean ITCZ position beginning at 180 ka, with a maximum at around 173 ka (Figure 4). Stable isotopes from an Arabian Sea core suggest decreased salinities due to

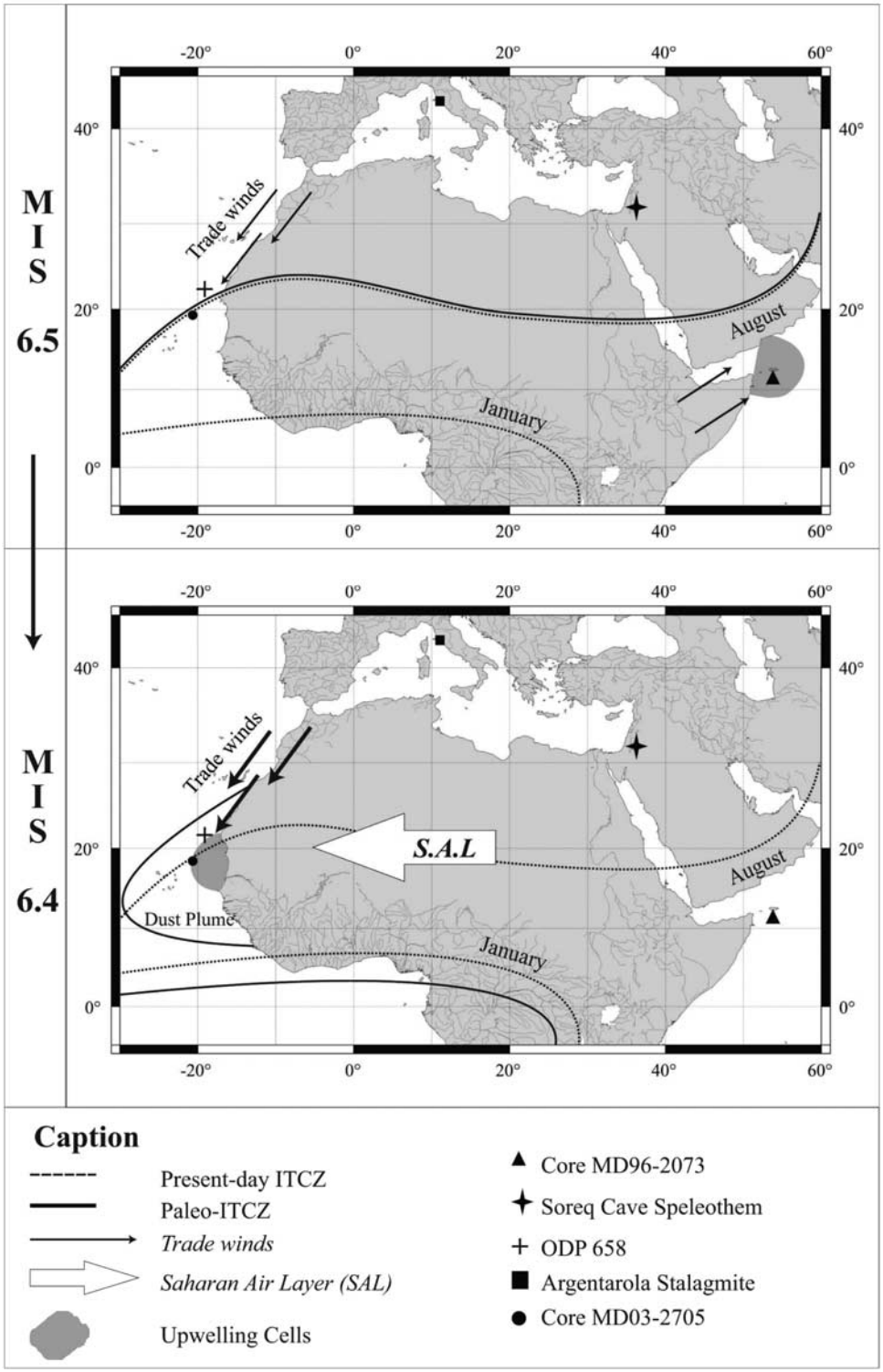

Figure 6. Conceptual model of the atmospheric and oceanic conditions during (top) MIS 6.5 and (bottom) MIS 6.4 around North Africa. The model is based from the results of five sites: the core MD03-2705 in the northwest subtropical Atlantic Ocean, the core ODP 658 in the northwest subtropical Atlantic Ocean [*Dupont and Hooghiemstra*, 1989], the Argentarola stalagmite on the Tyrrhenian coast of Italy [*Bard et al.*, 2002], the Soreq Cave speleothem in Israel [*Ayalon et al.*, 2002], and the core MD96-2073 in the NW Indian Ocean [*Malaizé et al.*, 2006] (see caption).

increased precipitation together with increased southwest monsoon wind strength. Such events were linked to the same northward ITCZ migration for the same period of time [*Malaizé et al.*, 2006]. In core MD03-2705, the upwelling began decreasing and SST began increasing at 180 ka. Both reached a plateau at 173 ka implying wind strength decreased from 176 to 168 ka. Changes in the atmospheric and oceanic monsoons were synchronous or nearly so within the Mauritanian and Socotran basin, i.e., on both sides of the African continent, and occurred when precession is minimum and obliquity increases (Figure 4). Our observations confirm the hypothesis proposed by *Tuenter et al.* [2003], suggesting that low precession together with high obliquity favor a northward migration of the ITCZ over Africa.

[41] The δ^{18}O isotopic records obtained from speleothems around the Mediterranean Sea shifted to more negative values (implying higher precipitation) between 182 and 175 ka for the Soreq Cave and between 180 and 170 ka for the Italian cave (Figure 4). Both records use ^{230}Th/U for dating. This interpretation is supported by the deposition of organic-rich layers called sapropels in the Eastern Mediterranean Sea, which are likely the result of increased Nile river discharge [e.g., *Rossignol-Strick*, 1983; *Bard et al.*, 2002]. The two speleothem records (Soreq speleothems and Argentarola stalagmite) are consistent with the interpretation of a northward migration of the ITCZ, which is in-phase and coherent with increased rainfall over North Africa and the Mediterranean basin during substage 6.5. Rainfall and North African upwelling are conversely interpreted to decrease in MIS 6.4 via the same mechanism (e.g., forced by Milankovitch insolation cycles).

[42] A northward relocation of the ITCZ over North Africa during MIS 6.5 has also been suggested by the study of the ODP core 658 [*Dupont and Hooghiemstra*, 1989]. Vegetation tracers such as the percentage of forest, grass and Cyperaceae pollen in ODP core 658 suggest a northward shift in the Sahara-Sahel boundary, consistent with a northward movement of the ITCZ during MIS 6.5. However, a substantial lag is observed between the timing of atmospheric and oceanic shifts, as detected by the $\Delta\delta^{18}$O, planktonic δ^{13}C and Ti/Al ratio in MD03-2705 and the vegetation response on the continent at the end of MIS 6.5. Reduced monsoon intensity in core MD03-2705 began 8 ka earlier that the southward migration of the vegetation belt. However, *Dupont and Hooghiemstra* [1989] present a lower-resolution record on ODP658 than our results. Consequently, some episodes in vegetation changes can be missed because of this low resolution, which might artificially suggest a lag of vegetation changes. According to *Dupont and Hooghiemstra* [1989], a weak southward migration in vegetation and presumably in precipitation took place between 175 and 167 ka. The pollen diagram indicates a decrease of ~10% in forest, grass and Cyperaceae pollen total.

[43] MIS 6.5 ended with the decline of high precipitation and the onset of drier conditions. The dust increase observed in core MD03-2705 during the glacial period requires increased aridity over the nearby continent. The abrupt rate of changes in humid/arid conditions over the continent (less than 1.3 ka) raises the question of linearity/nonlinearity in the environmental response to a gradual insolation forcing.

5.3. An Abrupt Continental Change Paradox?

[44] The new high resolution of eolian quartz records at the site MD03-2705 highlights the abrupt termination of the monsoonal MIS 6.5 near 168 ka B.P. This atmospheric transition apparently occurred within millennial time scales (1.3 ka) and probably less [e.g., *Cole et al.*, 2009], indicating an abrupt desertification of northern Africa. Moreover, a recent study led on the ODP658 core, which is nearby MD03-2705, suggests that during the Holocene two transitions between dry and humid conditions and between humid and dry conditions might have occurred in less than a few hundred years [*deMenocal et al.*, 2000; *Cole et al.*, 2009]. The limitation of the core MD03-2705 chronology does not allow the transition from humid to dry condition to be determined on less than a millennial scale. It might have occurred in century or in few decadal scales, as proposed in the ODP658 results by *Cole et al.* [2009]. The transition between MIS 6.5 and MIS 6.4 cannot be explained by a linear response to the gradual reduction in summer insolation forcing. According to previous studies based on paleodata and climate models focusing on the last climatic cycle, we suggest that two positive feedback processes at the end of the MIS 6.5 monsoon period, related to vegetation-albedo effects and sea surface temperatures, contributed to this rapid wet to dry transition.

[45] Rapid climate changes recorded in core MD03-2705 between MIS 6.5 and MIS 6.4 might also be compared to rapid environmental changes during the Holocene. During this period, an "African humid period" (AHP) has been detected especially in North Africa, where the paleoclimatological reconstructions reveal more humid conditions than today [*Adkins et al.*, 2006]. Climate models show enhance in monsoon activity to be the principal source of the AHP, with increases in tropical rainfall over southern Asia and North Africa that coincide with the precessional summer insolation maximum. *Prell and Kutzbach* [1987] suggest a linear relationship between tropical climate and orbital forcing. However, this linear response between isolation and precipitation anomalies could not explain the abrupt increases observed in lake level during the AHP. Moreover, *deMenocal et al.* [2000] show an abrupt dust onset off of Africa at the end of the AHP. These abrupt African climate responses to insolation forcing contradict the linear response suggested by *Prell and Kutzbach* [1987]. The mechanisms of the nonlinear climate sensitivity based on the CLIMBER2 model proposed by *Charney* [1975] and *Claussen et al.* [1999] suggest that the feedback processes could come from vegetation and ocean temperature feedbacks [*deMenocal et al.*, 2000]. This climate system model of intermediate complexity is based on the ocean-atmosphere-vegetation CLIMBER model that includes dynamic vegetation responses to surface climate changes. Previously, *Ganopolski et al.* [1998] report the application of CLIMBER model and the results suggest that subtropics were strongly affected by a vegetation-precipitation positive feedback. By examining the new results from this model (global climate-terrestrial ecosystem model coupled to an atmosphere-ocean-dynamic

vegetation model (FOAM)) including a more complex vegetation simulation, *Liu et al.* [2007] suggest that the monsoon system at the mid-Holocene would not collapse suddenly in spite of a diminished vegetation. This new view highlights the link between vegetation evolution and dust accumulation (e.g., the reduction of the plants implying a desertification of the soil). The precipitation does not diverge from the precessional forcing. This important point suggests that the monsoon enhancement and the average position of the ITCZ are not governed by the same mechanisms and show a nonlinear response between each other.

[46] We can suggest that the increased dust flux during the transition MIS 6.5 and 6.4 in our marine sediment is consistent with a major vegetation collapse. An abrupt sea surface cooling with an intensification of the coastal upwelling occurred during the winter monsoon of the MIS 6.4. Such environmental changes could trigger feedbacks which could explain such rapid changes.

[47] Other studies have described rapid southward migration of the ITCZ during cold events, during the last glacial period, such as Heinrich events [*Jullien et al.*, 2007]. *Jullien et al.* [2007] hypothesized that during these cold events, intensified African dust supplies should be associated with a southward shifted ITCZ. Increased eolian dust delivery is indeed observed during MIS 6.4 in core MD03-2705 (Figure 6). The simultaneous aridity signals off both sides of North Africa during MIS 6.4 would suggest an abrupt tropical atmosphere reorganization and coherent southward shift of the ITCZ [*Mulitza et al.*, 2008] (Figure 6).

5.4. Global Impacts

[48] Recent multiproxy reconstructions of the Arabian Sea summer monsoon intensity have suggested a southward shift of the ITCZ during periods of rapid shifts to colder climate at millennial scale during the last glacial period [*Ivanochko et al.*, 2005] or for the MIS 6.5 to MIS 6.4 transition [*Malaizé et al.*, 2006]. Comparing their multiproxy reconstruction with other tropical paleorecords and Greenland ice core records, the authors suggest that reduced low-latitude convection resulting from a southward shifted ITCZ could reduce humidity throughout the tropics and have global consequences [*Ivanochko et al.*, 2005]. Conversely, during interstadials, expanded tropical convection is suggested to have increased tropical humidity and temperature affecting heat transfer from the tropics to the extratropics and subpolar latitudes [*Ivanochko et al.*, 2005]. Modeling studies [*Van Huissteden*, 2004] have demonstrated the possible importance of a biogenic positive climate feedback in increased methanogenesis from permafrost areas once high-latitude warming commences. On the glacial/interglacial time scale, this biogenic feedback is likely to be important and is probably related to the methane (CH_4) concentration changes also observed in GISP2 or Byrd ice core records [*Brook et al.*, 1996; *Blunier et al.*, 1998]. Studies suggest that changes in tropical convection could affect stadial/interstadial shifts in CH_4 emissions from northern wetlands [*Ivanochko et al.*, 2005].

[49] Some increases in atmospheric CH_4 could be expected in ice cores during MIS 6.5. A high-resolution atmospheric record of the penultimate deglaciation are available from the Dome C–EPICA ice core and shows a significant increase in CH_4 concentration between 188 and 169 ka [*Loulergue et al.*, 2008], supporting the previous Vostok ice core records [*Petit et al.*, 1999; *Delmotte et al.*, 2004]. At least three peaks in the CH_4 record have been revealed within the MIS 6.5 time interval. As suggested by the authors, these millennial methane events could be linked to a dominant contribution of monsoon related processes [*Loulergue et al.*, 2008]. Moreover three strong minima from $\delta^{18}O$ records of Chinese speleothem during the MIS 6.5 suggest rapid atmospheric events linked to strong precipitation within low-latitude band [*Wang et al.*, 2008]. Following *Ivanochko et al.* [2005], we argue that these CH_4 increases could be linked to intensified tropical convection during substage 6.5, leading to an increase in overall tropical humidity and temperature, and ultimately increased CH_4 concentration. The abrupt drop in monsoon intensity during MIS 6.4 could have an opposite consequence, decreasing the relative humidity and temperature over the tropics, and ultimately leading to a decrease in the atmospheric methane.

[50] Maximum values in the isotopic composition of atmospheric oxygen ($\delta^{18}O_{atm}$) have also been observed during MIS 6.5, centered around 175 ka [*Mélières et al.*, 1997; *Malaizé et al.*, 1999]. This peak in the $\delta^{18}O_{atm}$ record leads to an exceptional minimum in the so-called Dole effect, which is the difference between atmospheric and oceanic $\delta^{18}O$ values [*Bender et al.*, 1994]. Changes in the global photosynthesis/respiration balance or modification of the hydrological cycle have been proposed as possible explanations of the $\delta^{18}O_{atm}$ record [*Hoffmann et al.*, 2004]. Enhancement of the strength of the tropical convection zones, leading to an increase in tropical humidity during MIS 6.5, as described by our marine record, could be the answer to such changes in the global $\delta^{18}O_{atm}$, i.e., to the global Dole effect. Such a link between strong summer East Asian Monsoon and the global $\delta^{18}O_{atm}$ record has recently been revealed over the past 224,000 years [*Wang et al.*, 2008].

6. Conclusions

[51] The multiple proxies investigated in this study provide new insights into the paleoclimatology of marine isotopic substage 6.5 and the transition between MIS 6.5 and MIS 6.4 over the North African and Mediterranean basins. The high-resolution isotopic and sediment studies (including the analyses on thin sections) performed on archives from the northwest African margin document an evolution of the African monsoon during MIS 6 and more particularly between MIS 6.5 (wet period) and MIS 6.4 (dry period). Weak upwelling and high SSTs are suggested at 175 ka by the planktonic $\delta^{13}C$ record and benthic-planktonic $\delta^{18}O$ anomalies; this could be related to a strong northward shifted ITCZ. MIS 6.5 was characterized by "warmer" and weaker atmospheric circulation conditions compared with the whole MIS 6 record. An abrupt southward shift of the ITCZ during MIS 6.4 caused a decrease in the monsoon influence and favored eolian supply of conti-

nental dust via strengthened SAL winds. The latitudinal position of the ITCZ is hypothesized to result from a combined forcing of both precession and obliquity. Our results support the model results of *Tuenter et al.* [2003], adding new evidence from the northwest coast of Africa to the Arabian Sea records obtained by *Malaizé et al.* [2006].

[52] Abrupt changes observed over the continent are too rapid to be a linear response to a gradual insolation forcing. Taking into account studies on similar rapid changes over North Africa for the last climatic cycle, we explain such rapid evolution by positive feedbacks of continental vegetation and marine SST changes.

[53] Following previous work, we suggest that strong northwest African summer monsoons might be associated with changes in the tropical hydrological cycle and atmospheric convection, increasing tropical and extratropical temperatures and possibly contributing to changes in CH_4 greenhouse gas emissions, together with a minimum in the $\delta^{18}O_{atm}$, affecting the global Dole effect.

[54] **Acknowledgments.** We thank Frederique Eynaud and Philippe Martinez for their help and stimulating discussions and Olivier Ther, Bernard Martin, and Joel Saint-Paul for the preparation of the samples and the thin sections. We would like to thank Ralph Schneider for his analysis of the XRF data set. Thanks are due to Justin Wettstein and William Fletcher for their assistance with language. We are grateful for the constructive comments and suggestions from Editor Eelco Rohling and the associate editor Jess Adkins and the reviews of Tara Ivanochko and an anonymous reviewer, which have improved this paper. The sediment core MD03-2705 is a part of the international program IMAGES. It has been collected thanks to the staff of the research vessel *Marion Dufresne*, supported by the French agencies Ministère de l'Education Nationale de la Recherche et de la Technologie, Centre National de la Recherche Scientifique (CNRS), and Institut Paul Emile Victor. Financial contribution from the ECLIPSE program, the ANR program called PICC, and the LEFE-EVE program called MOMIES is acknowledged. This paper is contribution 1686 of Bordeaux 1 University, EPOC, UMR5805 CNRS.

References

Adkins, J., P. deMenocal, and G. Eshel (2006), The "African humid period" and the record of marine upwelling from excess ^{230}Th in Ocean Drilling Program Hole 658C, *Paleoceanography*, *21*, PA4203, doi:10.1029/2005PA001200.

Ayalon, A., M. Bar-Matthews, and A. Kaufman (2002), Climatic conditions during marine oxygen isotope stage 6 in the eastern Mediterranean region from the isotopic composition of speleothems of Soreq Cave, Israel, *Geology*, *30*, 303–306, doi:10.1130/0091-7613(2002)030<0303:CCDMOI>2.0.CO;2.

Bard, E., G. Delaygue, F. Rostek, F. Antonioli, S. Silenzi, and D. P. Schrag (2002), Hydrological conditions over the western Mediterranean basin during the deposition of the cold sapropel 6 (ca. 175 kyr BP), *Earth Planet. Sci. Lett.*, *202*, 481–494, doi:10.1016/S0012-821X(02)00788-4.

Beltagy, A. I., R. Chester, and R. C. Padgham (1972), The particle-size distribution of quartz in some North Atlantic deep-sea sediments, *Mar. Geol.*, *13*, 297–310, doi:10.1016/0025-3227(72)90012-6.

Bender, M., T. Sowers, and L. Labeyrie (1994), The Dole effect and its variations during the last 130,000 years as measured in the Vostok ice core, *Global Biogeochem. Cycles*, *8*(3), 363–376, doi:10.1029/94GB00724.

Blunier, T., et al. (1998), Asynchrony of Antarctic and Greenland climate change during the last glacial period, *Nature*, *394*, 739–743, doi:10.1038/29447.

Boyle, E. A. (1983), Chemical accumulation variations under the Peru current during the past 130,000 years, *J. Geophys. Res.*, *88*(C12), 7667–7680, doi:10.1029/JC088iC12p07667.

Broccoli, A. J., K. A. Dahl, and R. J. Stouffer (2006), Response of the ITCZ to Northern Hemisphere cooling, *Geophys. Res. Lett.*, *33*, L01702, doi:10.1029/2005GL024546.

Brook, E., T. Sowers, and J. Orchardo (1996), Rapid variations in atmospheric methane concentration during the past 110,000 years, *Science*, *273*(5278), 1087–1091, doi:10.1126/science.273.5278.1087.

Calvert, S. E., T. F. Pedersen, and R. E. Karlin (2001), Geochemical and isotopic evidence for post-glacial palaeoceanographic changes in Saanich Inlet, British Columbia, *Mar. Geol.*, *174*, 287–305, doi:10.1016/S0025-3227(00)00156-0.

Charney, J. G. (1975), Dynamics of deserts and drought in the Sahel, *Q. J. R. Meteorol. Soc.*, *101*(428), 193–202, doi:10.1002/qj.49710142802.

Cheddadi, R., and M. Rossignol-Strick (1995), Eastern Mediterranean Quaternary paleoclimates from pollen and isotope records of marine cores in the Nile Cone area, *Paleoceanography*, *10*, 291–300, doi:10.1029/94PA02672.

Claussen, M., C. Kubatzki, V. Brovkin, A. Ganopolski, P. Hoelzmann, and H.-J. Pachur (1999), Simulation of an abrupt change in Saharan vegetation in the mid-Holocene, *Geophys. Res. Lett.*, *26*(14), 2037–2040, doi:10.1029/1999GL900494.

Cole, J. M., S. L. Goldstein, P. B. deMenocal, and S. R. Hemming (2009), Contrasting compositions of Saharan dust in the eastern Atlantic Ocean during the last deglaciation and African humid period, *Earth Planet. Sci. Lett.*, *278*, 257–266, doi:10.1016/j.epsl.2008.12.011.

Cramp, A., and G. O'Sullivan (1999), Neogene sapropels in the Mediterranean: A review, *Mar. Geol.*, *153*, 11–28, doi:10.1016/S0025-3227(98)00092-9.

Curry, W. B., J. C. Duplessy, L. D. Labeyrie, and N. J. Shackleton (1988), Changes in the distribution of the δ^{13}C of deep water ΣCO_2 between the last glaciation and the Holocene, *Paleoceanography*, *3*, 317–342, doi:10.1029/PA003i003p00317.

Delmotte, M., J. Chappellaz, E. Brook, P. Yiou, J. M. Barnola, C. Goujon, D. Raynaud, and V. I. Lipenkov (2004), Atmospheric methane during the last four glacial-interglacial cycles: Rapid changes and their link with Antarctic temperature, *J. Geophys. Res.*, *109*, D12104, doi:10.1029/2003JD004417.

deMenocal, P. B. (1995), Plio-Pleistocene African climate, *Science*, *270*(5233), 53–59, doi:10.1126/science.270.5233.53.

deMenocal, P. B. (2004), African climate change and faunal evolution during the Pliocene-Pleistocene, *Earth Planet. Sci. Lett.*, *220*, 3–24, doi:10.1016/S0012-821X(04)00003-2.

deMenocal, P. B., J. Ortiz, T. Guilderson, J. Adkins, M. Sarnthein, L. Baker, and M. Yarusinsky (2000), Abrupt onset and termination of the African humid period: Rapid climate responses to gradual insolation forcing, *Quat. Sci. Rev.*, *19*, 347–361, doi:10.1016/S0277-3791(99)00081-5.

Ding, Z. L., J. Z. Ren, S. L. Yang, and T. S. Liu (1999), Climate instability during the penultimate glaciation: Evidence from two high-resolution loess records, China, *J. Geophys. Res.*, *104*(B9), 20,123–20,132, doi:10.1029/1999JB900183.

Duplessy, J.-C., L. Labeyrie, A. Juillet-Leclerc, F. Maitre, J. Duprat, and M. Sarnthein (1991), Surface salinity reconstruction of the North Atlantic Ocean during the Last Glacial Maximum, *Oceanol. Acta*, *14*, 311–324.

Dupont, L. M., and H. Hooghiemstra (1989), The Saharan-Sahelian boundary during the Brunhes chron., *Acta Bot. Neerl.*, *38*, 405–415.

Ganopolski, A., C. Kubatzki, M. Claussen, V. Brovkin, and V. Petoukhov (1998), The influence of vegetation-atmosphere-ocean interaction on climate during the mid-Holocene, *Science*, *280*(5371), 1916–1919, doi:10.1126/science.280.5371.1916.

Gasse, F. (2000), Hydrological changes in the African tropics since the Last Glacial Maximum, *Quat. Sci. Rev.*, *19*, 189–211, doi:10.1016/S0277-3791(99)00061-X.

Glaccum, R. A., and J. M. Prospero (1980), Sahara aerosols over the tropical North Atlantic mineralogy, *Mar. Geol.*, *37*, 295–321, doi:10.1016/0025-3227(80)90107-3.

Grousset, F. E., and P. E. Biscaye (2005), Tracing dust sources and transport patterns using Sr, Nd and Pb isotopes, *Chem. Geol.*, *222*(3–4), 149–167, doi:10.1016/j.chemgeo.2005.05.006.

Guichard, S., F. Jorissen, and J.-P. Peypouquet (1999), Late Quaternary benthic foraminiferal records testifying lateral variability of the Cape Blanc upwelling signal, *C. R. Acad. Sci., Ser. IIA Sci. Terre Planetes*, *329*(4), 295–301, doi:10.1016/S1251-8050(99)80249-3.

Hoffmann, G., et al. (2004), A model of the Earth's Dole effect, *Global Biogeochem. Cycles*, *18*, GB1008, doi:10.1029/2003GB002059.

Holz, C. (2004), Climate-induced variability of fluvial and aeolian sediment supply and gravity-driven sediment transport off northwest Africa, Ph.D. dissertation, 129 pp., Univ. of Bremen, Bremen, Germany.

Hughes, P., and E. D. Barton (1974), Physical investigations in the upwelling region of northwest Africa on RRS Discovery cruise 48, *Tethys*, *6*, 43–52.

Huelsemann, J. (1966), On the routine analysis of carbonates in unconsolidated sediments, *J. Sediment. Petrol.*, *36*(2), 622–625.

Husar, R. B., J. M. Prospero, and L. L. Stowe (1997), Characterization of tropospheric aerosols over the oceans with the NOAA advanced very high resolution radiometer optical thickness operational product, *J. Geophys. Res.*, *102*(D14), 16,889–16,909, doi:10.1029/96JD04009.

Imbrie, J., J. Hays, D. G. Martinson, A. McIntyre, A. C. Mix, J. J. Morley, N. G. Pisias, W. L. Prell, and N. J. Shackleton (1984), The orbital theory of Pleistocene climate: Support from a revised chronology of the marine ^{18}O record, in *Milankovitch and Climate*, edited by A. Berger et al., pp. 269–305, Kluwer Acad., Dordrecht, Netherlands.

Ivanochko, T., R. Ganeshram, G.-J. Brummer, G. Ganssen, S. Jung, S. Moreton, and D. Kroon (2005), Variations in tropical convection as an amplifier of global climate change at the millennial scale, *Earth Planet. Sci. Lett.*, *235*, 302–314, doi:10.1016/j.epsl.2005.04.002.

Jansen, J. H. F., S. J. Van der Gaast, B. Koster, and A. J. Vaars (1998), CORTEX: A shipboard XRF-scanner for element analyses in split sediment cores, *Mar. Geol.*, *151*, 143–153, doi:10.1016/S0025-3227(98)00074-7.

Jouzel, J., et al. (2007), Orbital and millennial Antarctic climate variability over the past 800,000 years, *Science*, *317*(5839), 793–796, doi:10.1126/science.1141038.

Jullien, E., et al. (2007), Low-latitude "dusty events" vs. high-latitude "icy Heinrich events,", *Quat. Res.*, *68*(3), 379–386, doi:10.1016/j.yqres.2007.07.007.

Kim, S.-T., and J. R. O'Neil (1997), Equilibrium and nonequilibrium oxygen isotope effects in synthetic carbonates, *Geochim. Cosmochim. Acta*, *61*(16), 3461–3475, doi:10.1016/S0016-7037(97)00169-5.

Lambert, F., B. Delmonte, J. R. Petit, M. Bigler, P. R. Kaufmann, M. A. Hutterli, T. F. Stocker, U. Ruth, J. P. Steffensen, and V. Maggi (2008), Dust-climate couplings over the past 800,000 years from the EPICA Dome C ice core, *Nature*, *452*, 616–619, doi:10.1038/nature06763.

Levitus, S., and T. P. Boyer (1994), *World Ocean Atlas 1994*, vol. 4, *Temperature, NOAA Atlas NESDIS*, vol. 4, 129 pp., NOAA, Silver Spring, Md.

Levitus, S., R. Burgett, and T. P. Boyer (1994), *World Ocean Atlas 1994*, vol. 3, *Salinity, NOAA Atlas NESDIS*, vol. 3, 111 pp., NOAA, Silver Spring, Md.

Lisiecki, L. E., and M. E. Raymo (2005), A Pliocene-Pleistocene stack of 57 globally distributed benthic $\delta^{18}O$ records, *Paleoceanography*, *20*, PA1003, doi:10.1029/2004PA001071.

Liu, Z., et al. (2007), Simulating the transient evolution and abrupt change of northern Africa atmosphere-ocean-terrestrial ecosystem in the Holocene, *Quat. Sci. Rev.*, *26*, 1818–1837, doi:10.1016/j.quascirev.2007.03.002.

Loulergue, L., A. Schilt, R. Spahni, V. Masson-Delmotte, T. Blunier, B. Lemieux, J.-M. Barnola, D. Raynaud, T. Stocker, and J. Chappellaz (2008), Orbital and millennial-scale features of atmospheric CH_4 over the past 800,000 years, *Nature*, *453*, 383–386, doi:10.1038/nature06950.

Mackensen, A., and T. Bickert (1999), Stable carbon isotopes in benthic foraminifera: Proxies for deep and bottom water circulation and new production, in *Use of Proxies in Paleoceanography: Examples From the South Atlantic*, edited by G. Fisher and G. Wefer, pp. 229–254, Springer, Berlin.

Malaizé, B., D. Paillard, J. Jouzel, and D. Raynaud (1999), The Dole effect over the last two glacial-interglacial cycles, *J. Geophys. Res.*, *104*(D12), 14,199–14,208, doi:10.1029/1999JD900116.

Malaizé, B., C. Joly, M. T. Vénec-Peyré, F. Bassinot, N. Caillon, and K. Charlier (2006), Phase lag between Intertropical Convergence Zone migration and subtropical monsoon onset over the northwestern Indian Ocean during marine isotopic substage 6.5 (MIS 6.5), *Geochem. Geophys. Geosyst.*, *7*, Q12N08, doi:10.1029/2006GC001353.

Martinez, P., P. Bertrand, G. B. Shimmield, K. Cochrane, F. J. Jorissens, J. Foster, and M. Dignan (1999), Upwelling intensity and ocean productivity changes off Cap Blanc (northwest Africa) during the last 70,000 years: Geochemical and micropalaeontological evidence, *Mar. Geol.*, *158*, 57–74, doi:10.1016/S0025-3227(98)00161-3.

Matthewson, A. P., G. B. Shimmield, D. Kroon, and A. E. Fallick (1995), A 300 kyr high-resolution aridity record of the North African continent, *Paleoceanography*, *10*, 677–692, doi:10.1029/94PA03348.

Mélières, M.-A., M. Rossignol-Strik, and B. Malaizé (1997), Relation between low latitude insolation and $\delta^{18}O$ change of atmospheric oxygen for the last 200 kyrs, as revealed by Mediterranean sapropels, *Geophys. Res. Lett.*, *24*(10), 1235–1238, doi:10.1029/97GL01025.

Migeon, S., O. Weber, J. C. Faugeres, and J. Saint-Paul (1999), SCOPIX: A new imaging system for core analysis, *Geo Mar. Lett.*, *18*, 251–255, doi:10.1007/s003670050076.

Mittelstaedt, E. (1983), The upwelling area off northwest Africa: A description of phenomena related to coastal upwelling, *Prog. Oceanogr.*, *12*, 307–331, doi:10.1016/0079-6611(83)90012-5.

Mittelstaedt, E. (1991), The ocean boundary along the northwest African coast: Circulation and oceanographic properties at the sea surface, *Prog. Oceanogr.*, *26*, 307–355, doi:10.1016/0079-6611(91)90011-A.

Molfino, B., and A. McIntyre (1990), Precessional forcing of nutricline dynamics in the equatorial Atlantic, *Science*, *249*(4970), 766–769, doi:10.1126/science.249.4970.766.

Moyes, J., J. Duplantier, J. Duprat, J. C. Faugères, C. Pujol, A. Pujos-Lamy, and J. P. Tastet (1979), Etude stratigraphique et sédimentologique, in *Géochimie Organique des Sédiments Marins Profonds*, pp. 121–213, Cent. Natl. de la Res. Sci., Paris.

Mulitza, S., M. Prange, J.-B. Stuut, M. Zabel, T. von Dobeneck, A. C. Itambi, J. Nizou, M. Schulz, and G. Wefer (2008), Sahel megadroughts triggered by glacial slowdowns of Atlantic meridional overturning, *Paleoceanography*, *23*, PA4206, doi:10.1029/2008PA001637.

Muller, G., and M. Gatsner (1971), Chemical analysis, *Neues Jahrb. Mineral. Monatsh.*, *10*, 466–469.

Murgese, D. S., P. De Deckker, M. I. Spooner, and M. Young (2008), A 35,000 year record of changes in the eastern Indian Ocean offshore Sumatra, *Palaeogeogr. Palaeoclimatol. Palaeoecol.*, *265*, 195–213, doi:10.1016/j.palaeo.2008.06.001.

Nicholson, S. E. (1996), A review of climate dynamics and climate variability in eastern Africa, in *The Limnology, Climatology and Paleoclimatology of the East African Lakes*, edited by T. C. Johnson and E. O. Odada, pp. 25–56, Gordon and Breach, Amsterdam.

O'Neil, J. R., R. N. Clayton, and T. K. Mayeda (1969), Oxygen isotope fractionation in divalent metal carbonates, *J. Chem. Phys.*, *51*, 5547–5558, doi:10.1063/1.1671982.

Paillard, D., L. Labeyrie, and P. Yiou (1996), Macintosh program performs time-series analysis, *Eos Trans. AGU*, *77*(39), 379, doi:10.1029/96EO00259.

Petit, J. R., et al. (1999), Climate and atmospheric history of the past 420,000 years from the Vostok ice core, Antarctica, *Nature*, *399*, 429–436, doi:10.1038/20859.

Prell, W. L., and J. E. Kutzbach (1987), Monsoon variability over the past 150,000 years, *J. Geophys. Res.*, *92*(D7), 8411–8425, doi:10.1029/JD092iD07p08411.

Ratmeyer, V., G. Fischer, and G. Wefer (1999), Lithogenic particle fluxes and grain size distributions in the deep ocean off northwest Africa: Implications for seasonal changes of aeolian dust input and downward transport, *Deep Sea Res., Part I*, *46*(8), 1289–1337, doi:10.1016/S0967-0637(99)00008-4.

Rossignol-Strick, M. (1983), African monsoons: An immediate climate response to orbital insolation, *Nature*, *304*, 46–49, doi:10.1038/304046a0.

Rossignol-Strick, M. (1985), Mediterranean Quaternary sapropels: An immediate response of the African monsoon to variation of insolation, *Palaeogeogr. Palaeoclimatol. Palaeoecol.*, *49*, 237–263, doi:10.1016/0031-0182(85)90056-2.

Rossignol-Strick, M., and M. Paterne (1999), A synthetic pollen record of the eastern Mediterranean sapropels of the last 1 Ma: Implications for the time-scale and formation of sapropels, *Mar. Geol.*, *153*, 221–237, doi:10.1016/S0025-3227(98)00080-2.

Schneider, R. R., P. J. Müller, and G. Wefer (1994), Late Quaternary paleoproductivity changes off the Congo deduced from stable carbon isotopes of planktonic foraminifera, *Palaeogeogr. Palaeoclimatol. Palaeoecol.*, *110*, 255–274, doi:10.1016/0031-0182(94)90087-6.

Schneider, R. R., B. Price, P. J. Müller, D. Kroon, and I. Alexander (1997), Monsoon related variations in Zaire (Congo) sediment load and influence of fluvial silicate supply on marine productivity in the east equatorial Atlantic during the last 200,000 years, *Paleoceanography*, *12*, 463–482, doi:10.1029/96PA03640.

Sirocko, F., D. Garbe-Schönberg, and B. Molfino (1996), Teleconnections between the subtropical monsoons and high-latitude climates during the last deglaciation, *Science*, *272*(5261), 526–529, doi:10.1126/science.272.5261.526.

Tiedemann, R. (1991), Acht millionen jahre klimageschichte von nordwest Afrika und paläozeanographie des angrenzenden Atlantiks: Hochauflösende Zeitreihen von ODP-sites 658–661, *Rep. 46*, 190 pp., Geol.-Palaeontol. Inst., Univ. of Kiel, Kiel, Germany.

Tiedemann, R., M. Sarnthein, and R. Stein (1989), Climatic changes in the western Sahara: Aeolo-marine sediment record of the last 8 million years (site 657–661), *Proc. Ocean Drill. Program Sci. Results*, *108*, 241–261.

Tsoar, H., and K. Pye (1987), Dust transport and the question of desert loess formation, *Sedimentology*, *34*, 139–153, doi:10.1111/j.1365-3091.1987.tb00566.x.

Tuenter, E., S. L. Weber, F. J. Hilgen, and L. J. Lourens (2003), The response of the African

summer monsoon to remote and local forcing due to precession and obliquity, *Global Planet. Change*, *36*(4), 219–235, doi:10.1016/S0921-8181(02)00196-0.

Van Camp, L., L. Nykjaer, E. Mittelstaedt, and P. Schlittenhardt (1991), Upwelling and boundary circulation off northwest Africa as depicted by infrared and visible satellite observations, *Prog. Oceanogr.*, *26*, 357–402, doi:10.1016/0079-6611(91)90012-B.

Van Huissteden, J. (2004), Methane emission from northern wetlands in Europe during oxygen isotope stage 3, *Quat. Sci. Rev.*, *23*, 1989–2005, doi:10.1016/j.quascirev.2004.02.015.

Vostok Project members (1995), Deciphering mysteries of past climate from Antarctic ice cores, *Earth Space*, *8*, 9.

Wang, Y., H. Cheng, R. L. Edwards, X. Kong, X. Shao, S. Chen, J. Wu, X. Jiang, X. Wang, and Z. An (2008), Millennial- and orbital-scale changes in the East Asian monsoon over the past 224,000 years, *Nature*, *451*, 1090–1093, doi:10.1038/nature06692.

Weaver, P. P. E., R. B. Wynn, N. H. Kenyon, and J. Evans (2000), Continental margin sedimentation, with special reference to the north-east Atlantic margin, *Sedimentology*, *47*, 239–256, doi:10.1046/j.1365-3091.2000.0470s1239.x.

Weldeab, S., D. Lea, R. Schneider, and N. Andersen (2007), 155,000 years of West African monsoon and ocean thermal evolution, *Science*, *316*(5829), 1303–1307, doi:10.1126/science.1140461.

Zaragosi, S., J.-F. Bourillet, F. Eynaud, S. Toucanne, B. Denhard, A. Van Toer, and V. Lanfumey (2006), The impact of the last European deglaciation on the deep-sea turbidite systems of the Celtic-Armorican margin (Bay of Biscay), *Geo Mar. Lett.*, *26*, 317–329, doi:10.1007/s00367-006-0048-9.

K. Charlier, F. Grousset, E. Jullien, B. Malaizé, and S. Zaragosi, Université Bordeaux 1, EPOC, UMR5805, CNRS, F-33405 Talence CEDEX, France.

A. Tisserand, Bjerknes Centre for Climate Research, Allégaten 70, N-5007 Bergen, Norway. (amandine.tisserand@bjerknes.uib.no)